Journal of Alloys and Compounds 494 (2010) 426–433

Contents lists available at ScienceDirect

Journal of Alloys and Compounds

journal homepage: www.elsevier.com/locate/jallcom

Grain refinement behavior of potassium fluozirconate (K_2ZrF_6) salts mixture introduced into Mg–10Gd–3Y magnesium alloy

Ming Sun[a,b], Guohua Wu[a,b,*], Jichun Dai[a,b], Wei Wang[a,b], Wenjiang Ding[a,b]

[a] National Engineering Research Center of Light Alloy Net Forming, Shanghai Jiaotong University, 800 Dongchuan Road, Shanghai 200240, China
[b] State Key Laboratory of Metal Matrix Composites, Shanghai Jiaotong University, Shanghai 200240, China

ARTICLE INFO

Article history:
Received 18 September 2009
Received in revised form 12 January 2010
Accepted 16 January 2010
Available online 25 January 2010

Keywords:
Mg–Gd–Y magnesium alloy
Zirconium
Potassium fluozirconate (K_2ZrF_6) salts mixture
Grain refinement
Inclusion

ABSTRACT

The influences of potassium fluozirconate (K_2ZrF_6) salts mixture (KSM) on the grain refinement, microstructure, mechanical properties and corrosion resistance of Mg–10Gd–3Y (GW103, wt.%) magnesium alloy were investigated. The results show that an addition of 8 wt.% KSM-2 (50 wt.% K_2ZrF_6–25 wt.% NaCl–25 wt.% KCl) provides the best combination of fine grain size and the lowest fraction of inclusions for GW103 alloy. The mechanical properties and corrosion resistance of GW103 alloy are improved by KSM-2 addition. The formation of Zr from the *in situ* reaction between Mg melt and K_2ZrF_6 is responsible for the refining mechanism of KSM. Compared with the Mg–30 wt.% Zr master alloy, the KSM refiner shows much longer fading time during smelting.

1. Introduction

In recent years, as weight reduction demands for automobile and aircraft body are becoming the world focus, magnesium alloys are becoming one of the key engineering materials due to their low density and high specific strength and stiffness [1–3]. It has been reported that the currently developed Mg–Gd–Y (GW)-based alloys are becoming the most promising heat-treating strengthen magnesium alloys [4], because they exhibit excellent specific strength both at room and elevated temperatures, which is higher than that of conventional Al and Mg alloys. Creep resistance of the Mg–Gd–Y-based alloys is markedly better than that of WE54 (Mg–5Y–2Nd–2HRE, wt.%), which is up to date the most creep resistant commercially available magnesium alloy [1,5–7].

Zirconium (Zr) is a powerful grain refiner for Mg–RE alloys. Addition of Zr leads to a fine and equiaxed microstructure, which is needed for structural uniformity and consistency in performance of Mg-products [8]. Zr addition and also leads to the improvement of mechanical properties and corrosion resistance [9–11]. The grain refining effect of zirconium was discovered by Sauerwald in Germany in the late 1940s [12], and later Emley proposed that the effect be based on the peritectic mechanism [13]. In the last 5 years, a lot of scientific papers have been published to describe the effect of Zr addition on the grain refinement of magnesium alloys [10,13–16].

As a grain refiner, the main introduction method is using commercial binary Mg–Zr master alloy, which contains Zr particles ranging from sub-micrometer to about 50 μm in size [17]. However, application of the Mg–Zr master alloy during industrial processing has some drawbacks. Firstly, Mg–Zr master alloys are most usually fabricated by a chemical reduction reaction between pure magnesium and salts mixture based on zirconium fluorides (ZrF_4) or zirconium chlorides ($ZrCl_4$) [18]. Since the process is technologically complicated and needs high energy inputs, modification of magnesium alloys by Zr addition significantly increases the price of alloys [19]. Secondly, $ZrCl_4$, as the main raw material for producing Mg–Zr, is easily volatile, deliquescent, and readily hydrolyzed, therefore unpleasant to use and difficult to store [20]. Thirdly, the utilization rate of Mg–Zr master alloy during alloying process is not satisfactory because that the undissolved Zr particles spontaneously settle due to the much higher density of Zr (6.52 g/cm^3) than liquid Mg [21], and that large zirconium particles (>5 μm) are inactive as nucleation centers [17]. On the contrary, substitution of $ZrCl_4$ by K_2ZrF_6 lowers the price, since the amount of zirconium in K_2ZrF_6 is lower than in $ZrCl_4$; moreover, the fluozirconate is non-volatile, stable in air and therefore can be easily stored and handled [20]. In other words, the above mentioned positive aspects are our main motivation to introduce Zr-rich salts mixture as a grain refiner in Mg alloys.

In the present study, the grain refinement effect of K_2ZrF_6 salts mixture (KSM) was investigated. The resulting mechanical properties and corrosion resistance of GW103K (where K means modification by Zr) alloy were studied as well.

* Corresponding author. Tel.: +86 21 54742630; fax: +86 21 34202794.
E-mail addresses: ghwu@sjtu.edu.cn, ghwu@sina.com (G. Wu).

0925-8388/$ – see front matter © 2010 Elsevier B.V. All rights reserved.
doi:10.1016/j.jallcom.2010.01.069

Table 1
The chemical compositions of KSM (wt.%).

Materials	K_2ZrF_6	NaCl	KCl
KSM-1	40	30	30
KSM-2	50	25	25
KSM-3	60	20	20

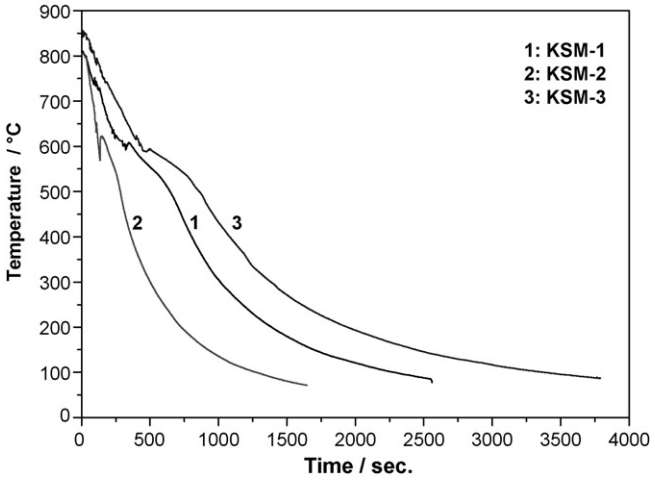

Fig. 1. Solidification curves of KSM.

2. Experimental procedure

2.1. Compositions of K_2ZrF_6 salts mixture (KSM)

K_2ZrF_6 is Zr-rich salt powder with melting point 840 °C. To avoid severe oxidation and burning of magnesium alloy (which smelting temperature is usually not higher than 800 °C), salts mixture to lower the melting temperature of K_2ZrF_6 must be used. The NaCl–KCl salt system is the base of the process that uses salt fluxes [22]. The fusion temperature of NaCl is 802 °C and that of KCl is 775 °C. However, the melting point of 50 wt.% NaCl–50 wt.% KCl system is only 658 °C [23]. Melting point of this mixture fulfills one of the requirements for a salt flux, namely the melting point is not too high to melt.

Three compositions of KSM used are shown in Table 1. The solidification curves of them are shown in Fig. 1, from which it can be seen that all the three melting points are not higher than 610 °C. So the salts mixture can melt during smelting.

2.2. Alloy smelting

Mg–10Gd–3Y (GW103) alloy was prepared from high purity Mg (99.95 wt.%) and master alloys of Mg–25 wt.% Gd and Mg–25 wt.% Y in an electric resistance furnace under a mixed flowing protective gas of CO_2 and SF_6 with the volume ratio of 100:1. After melting Mg and Mg–Gd, KSM was added into the melt at designed temperature accompanied by stirring. After holding for 30 min, Mg–Y was added, and then the melt was stirred again to get uniform distribution of various elements; finally, after designed holding time, cast at 750 °C into the metallic molds preheated to 150 °C. Usually, during smelting of GW103K alloy refined by Mg–Zr master alloy, Mg–Zr is added after melting of Mg–Y. In this work, the reason for KSM being added before Mg–Y is that Y can react with the K_2ZrF_6 and cause loss of Y.

2.3. Analysis methods

Zr contents in the alloys were determined by an inductively coupled plasma atomic emission spectroscopy (ICP-AES) analyzer. Specimens for microstructure observation were etched in a 4 vol.% nital. Microstructures were examined by an OLYMPUS BX51M optical microscope (OM), a JXA-8800R electron probe microanalyzer (EPMA) and a JEOL JSM-6460 scanning electron microscope (SEM). The compositions of inclusions were analyzed by energy dispersive spectroscope (EDS) attached to the SEM. Average grain size (AGS) was measured by linear intercept method in an OM. Phases were identified by Rigaku Dmax-rc X-ray diffractometer (XRD). Statistical volume fraction of inclusions (VF_i) in the alloy was measured with image software.

In order to obtain specimens without casting defects, all the tensile specimens were cut from the bottom of the ingots. The ambient temperature tensile tests were conducted on a Zwick/Roell Z020 universal material testing machine at a crosshead speed of 0.5 mm min^{-1}. The gage dimension of the specimens is 54.5 mm × 15 mm × 2.0 mm as shown in Fig. 2. Under the same conditions, various specimens were tested; presented values are average of at least three measurements.

The specimens for corrosion testing with dimension of ⌀35 mm × 4 mm were polished up to 800 grit, cleaned in ethanol and acetone and dried. Before immersion, the surface area (SA in cm^2) of the specimen was calculated and the weight (W_0 in mg) was measured. Corrosion resistance tests were carried out in a 5 wt.% NaCl aqueous solution (pH 8.3) at room temperature (25 ± 0.5 °C) for 3 days. After immersion time (t) of 3 days, the specimens were taken out and the corrosion products on the surface were removed in a chromic acid solution (200 g/L CrO_3 + 10 g/L $AgNO_3$ in water) at boiling condition for about 5 min. Following that the specimens were rinsed by distilled water and dried. The corrosion rate (CR) given as a weight loss per surface area and time (mg cm^{-2} day^{-1}) was calculated by the following equation: $CR = (W_0 - W_C)/(SA \times t)$. For every composition, various specimens were tested; presented values are average of at least three measurements.

3. Results

3.1. Effects of addition conditions on Zr content and Zr recovery

Fig. 3 shows the dependency of Zr content in GW103K alloy on the temperature of KSM addition; amount of 8% of KSM (wt.%) and holding time of 30 min were kept as constants. It can be seen that the Zr content increases with increasing temperature of KSM addition. The lower Zr content at 750 °C is related to the insufficient reaction between the magnesium and the K_2ZrF_6.

Fig. 4(a) shows the dependence of the Zr content in GW103K on the amount of added KSM (wt.%); temperature (780 °C) and holding time (30 min) are constant. It is obvious that resulting Zr content increases rapidly with the increasing KSM addition. At the same level of KSM addition, the obtained Zr content of KSM-1 processing is lower than that of KSM-2 and KSM-3 processing. Fig. 4(b) shows the relationship between the level of KSM addition and Zr recovery, where Zr recovery is defined as a Zr content in Fig. 4(a) divided by the initial Zr content in the corresponding KSM. It can be seen that with the increasing addition of KSM from 4 to 12% the Zr recov-

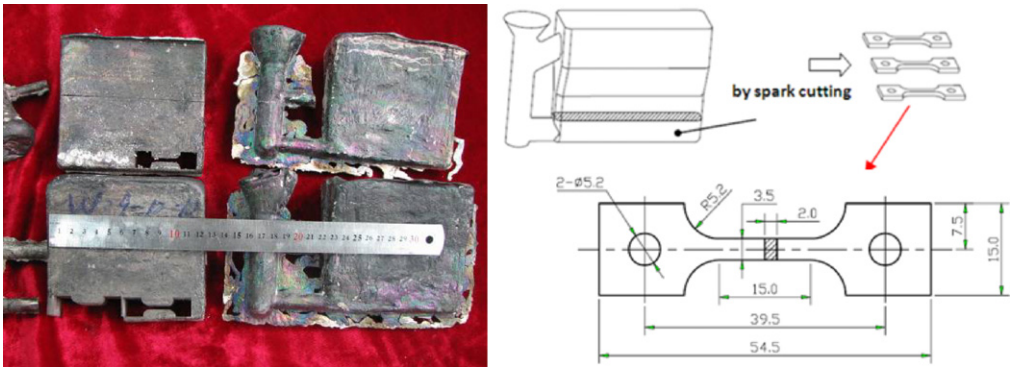

Fig. 2. Photo of the castings and gage dimension of rectangle tensile specimen.

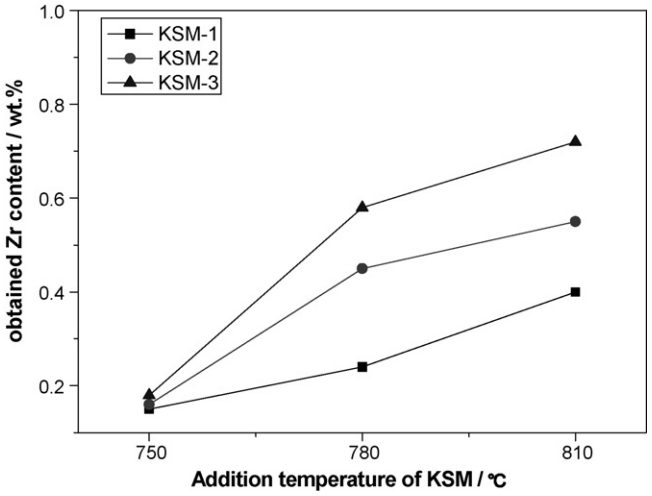

Fig. 3. Effect of addition temperature of 8% KSM on Zr content in GW103K alloy. Addition of 8% KSM and holding time of 30 min were kept as constants.

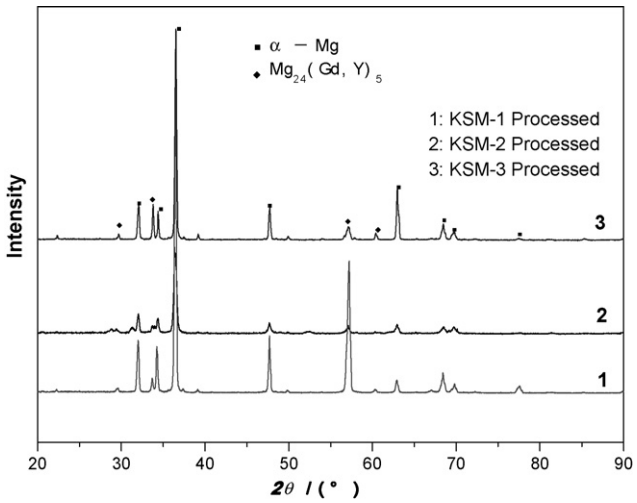

Fig. 5. XRD patterns of GW103K alloys.

ery decreases. Observed Zr recovery decreases due to the fact, that Zr in the KSM cannot be totally reduced by the chemical reaction. Even that the KSM addition in increasing, the increase rate of initial Zr amount in KSM is much faster than that of final Zr content in alloy.

3.2. Microstructure and grain refinement efficiency

XRD patterns of GW103K alloy as shown in Fig. 5 indicate that the alloy is composed from two phases, namely α-Mg and β-$Mg_{24}(Gd,Y)_5$. KSM addition does not lead to the formation of any new phase detectable by XRD.

Figs. 6–8 show the influence of KSM-1, KSM-2 and KSM-3 addition level on microstructure of GW103 alloy, respectively. The microstructures consist of the primary α-Mg matrix and β-$Mg_{24}(Gd,Y)_5$ phase, which distributes along the grain boundaries. It is clear that all three KSM have grain refinement ability, and with increasing addition level from 4 to 12% (wt.%), the AGS of GW103K alloy decreases gradually. However, as can be seen in above figures, with increasing KSM addition, the amount of inclusions in the microstructure increases.

The connection between the AGS and KSM addition is shown in Fig. 9, indicating that the grains become finer with the increase of KSM addition. The AGS with 12% KSM-2 addition is the finest (21 μm). Table 2 shows the volume fraction of inclusions (VF_i) in GW103K alloy with different KSM addition. At the same addition level, the VF_i increases with increasing the K_2ZrF_6 percentage in KSM. For every KSM, the VF_i increases with enhancing the addition level. Therefore, based on an overall consideration of the AGS and VF_i, the 8% KSM-2 provides the best combination of fine grain size and the lowest fraction of inclusions. Future research will be focused on the further decrease of inclusions amount in the microstructure of the 8% KSM-2.

Table 2
The volume fraction of inclusions in GW103K alloy with different KSM addition.

Refiner	4%	8%	12%
KSM-1	0.348%	0.617%	1.057%
KSM-2	0.488%	0.826%	1.103%
KSM-3	1.547%	2.287%	4.622%

Fig. 10 is an area scan by EPMA. It can be seen that Zr distribution is uniform, which is beneficial to the grain refinement effect. The presence of O results from the easy oxidization of Mg. Fig. 11 shows a characteristic SEM morphology and EDS analysis of the inclusion. EDS of the inclusion shows that its compositions are mainly O, F, Cl, Na, K, Mg, Gd, Y and Zr elements, indicating that it is composed of fluorides, chlorides and oxides; Gd and Y elements in the EDS analysis are obtained from the matrix. Reason for the presence of inclusions is possibly that the reaction products of KF and MgF_2 combine with the residual KSM to form clusters. This can be interpreted thanks to the relatively lower recovery efficiency of Zr (less than 50%) as shown in Fig. 4(b).

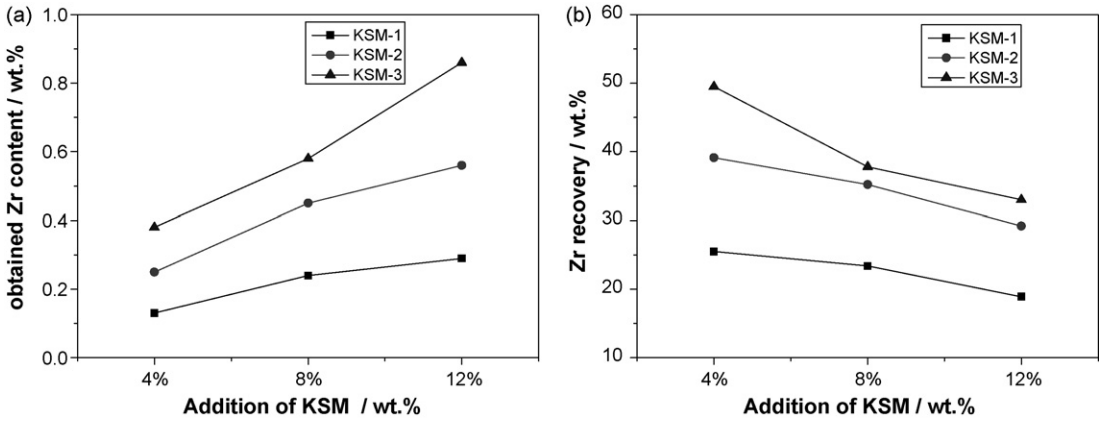

Fig. 4. Effect of addition level of KSM at 780 °C on (a) Zr content in GW103K alloy, and (b) Zr recovery. Temperature (780 °C) and holding time (30 min) are constant.

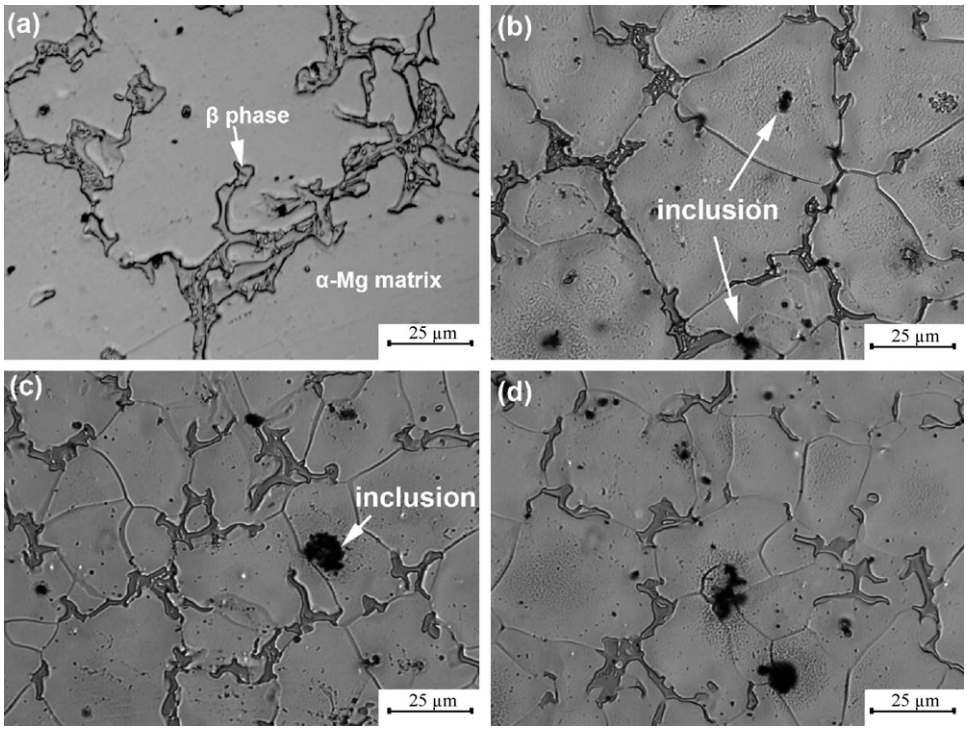

Fig. 6. Microstructure of GW103 alloy treated by KSM-1 with different addition level: (a) 0, (b) 4%, (c) 8% and (d) 12%.

3.3. Mechanical properties and corrosion resistance

The influence of KSM-2 addition on the mechanical properties is shown in Fig. 12. It is obvious that the ultimate tensile strength (UTS), the tensile yield strength (TYS) and the elongation (EL) all increase with increasing KSM-2 from 0 to 8%, and then decrease with KSM-2 addition from 8 to 12%. For 8% KSM-2 processed alloy, the tensile properties reach to the highest as UTS 162.4 MPa, TYS 140.9 MPa and EL 1.37%. The improvement of tensile properties is related to the Zr grain refinement.

Fig. 13 shows the corrosion rate in 5 wt.% NaCl solution. The corrosion rate decreases linearly with KSM-2 addition from 0 to

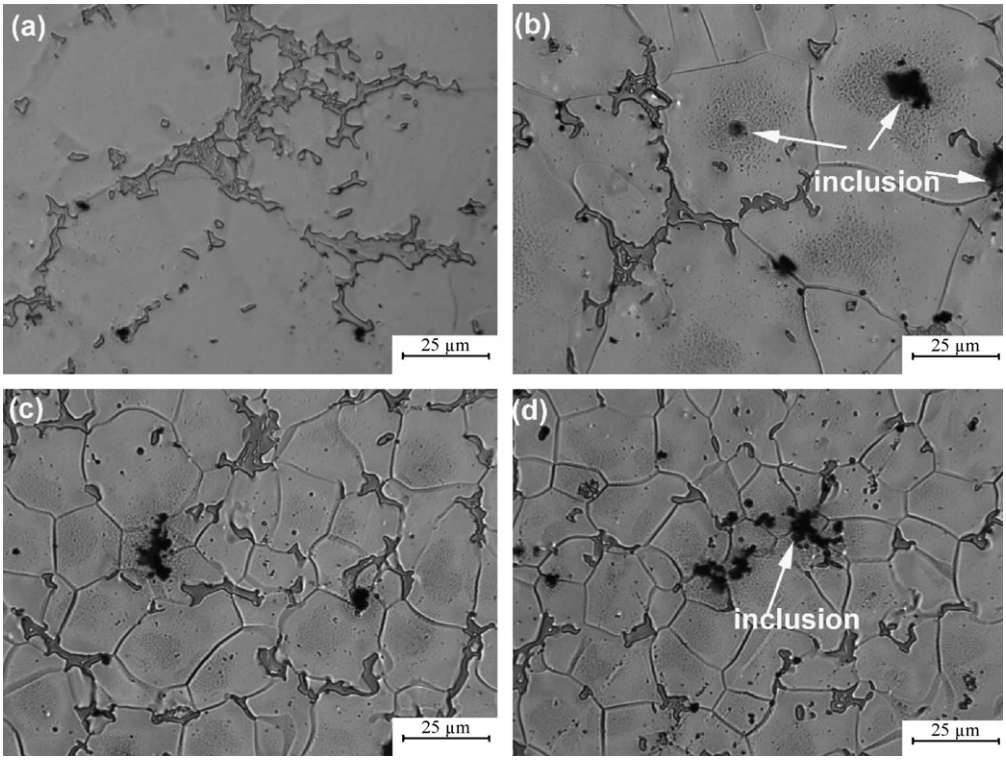

Fig. 7. Microstructure of GW103 alloy treated by KSM-2 with different addition level: (a) 0, (b) 4%, (c) 8% and (d) 12%.

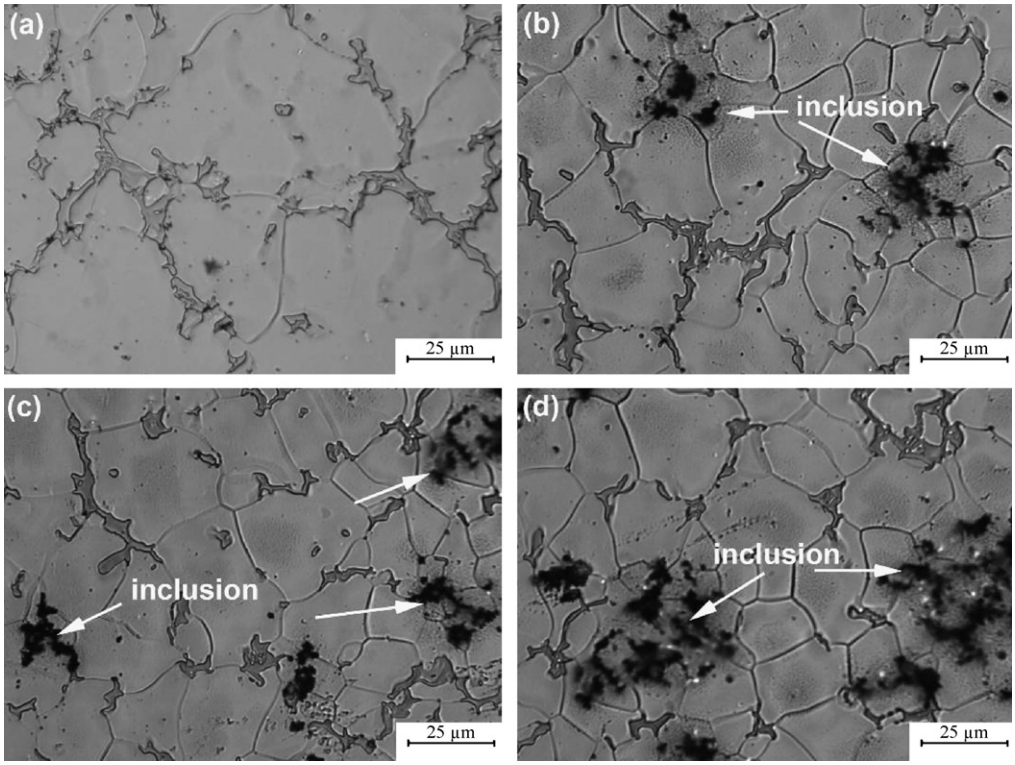

Fig. 8. Microstructure of GW103 alloy treated by KSM-3 with different addition level: (a) 0, (b) 4%, (c) 8% and (d) 12%.

8%, which is related to that Zr addition can improve corrosion resistance of the magnesium alloys [10]. On the other hand, the corrosion rate increases with KSM-2 addition from 8 to 12%. This is because the higher inclusion volume fraction deteriorates the corrosion resistance. It is well known that inclusions are creating discontinuities in the matrix with subsequent localization of high stress concentrations, which may act as a crack or void nucleation sites and thus may seriously damage the mechanical properties and corrosion resistance [24].

Fig. 14 shows the surface features of the corroded specimens after the immersion tests in 5% NaCl solution and removal of the corrosion products. It can be seen that the three specimens with KSM-2 addition all have less corrosion area than the base alloy. However, there are deep corrosion pits on the specimen with 12% KSM-2 processing. This is in good agreement with the change of corrosion rate shown in Fig. 13.

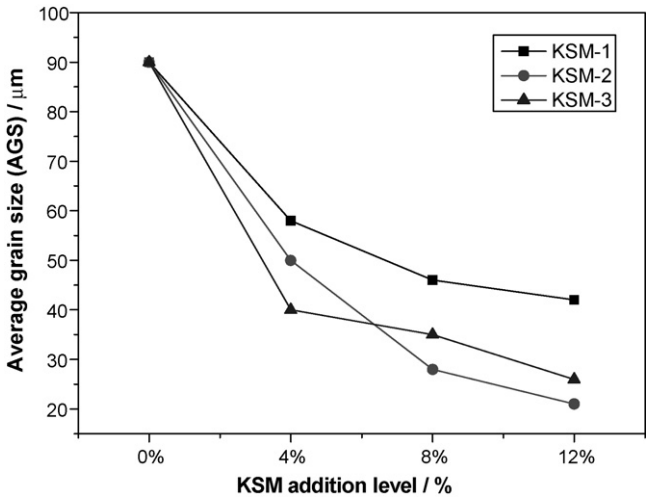

Fig. 9. Relationship between KSM addition level and AGS of GW103K alloy.

4. Discussion

GW103 magnesium alloy is grain-refined by K_2ZrF_6 salts mixture. Here, the refining mechanism is due to the formation of Zr. In the classical mechanism of grain refinement where Zr is added into magnesium alloy (introduced by Emley [13]), the primary Zr particles are segregated in the matrix at temperatures a little above the peritectic temperature. Due to the similarity of the lattices and the atomic sizes of magnesium and Zr, Zr particles serve as nucleation sites. However, evidence has recently been produced to show that Zr particles, precipitating from the melt or exist in the melt well above the peritectic temperature, can effectively nucleate magnesium grains [25]. In addition, slightly large Zr particles are fundamentally more effective as nucleants than small particles providing their settling velocity is slow [26]. The K_2ZrF_6 approach used in this work produces a large number of fresh Zr particles at the reduction temperature (780 °C). These Zr particles helped to deliver the excellent grain refinement observed in conjunction with those Zr particles that precipitated from the melt above the peritectic temperature during cooling. The dissolved Zr facilitates the refinement from a growth restriction perspective.

As a matter of fact, K_2ZrF_6 undergoes a peritectic melting at a temperature of 592 °C as Eq. (1) [27]:

$$K_2ZrF_6 \rightarrow xL(KF, ZrF_4) + yK_3ZrF_7 \quad (1)$$

Thus, at the experimental temperature (780 °C) and due to the easily melting of salts mixture, K_2ZrF_6 is totally decomposed into a mixture of a liquid phase (L) and K_3ZrF_7, where $L(KF, ZrF_4)$ is the liquid in equilibrium with K_3ZrF_7 at 700 °C in the KF–ZrF_4 phase diagram and $x + y = 1$ [27]. The decomposition could be balanced as follow:

$$2K_2ZrF_6 = L(KF, ZrF_4) + K_3ZrF_7 \quad (2)$$

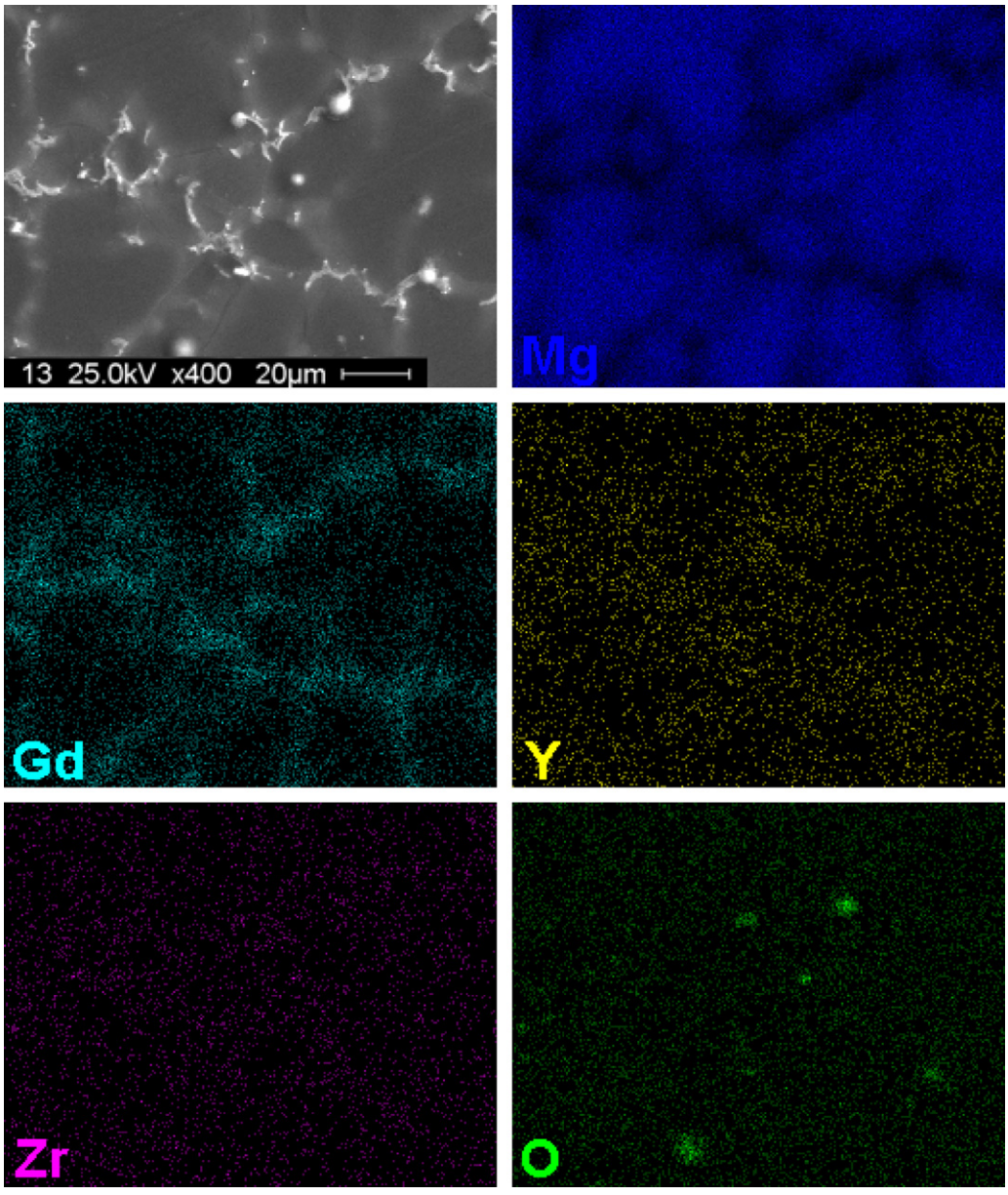

Fig. 10. EPMA morphology and surface distribution of the element Mg, Gd, Y, Zr, O of the 8% KSM-2 processed sample.

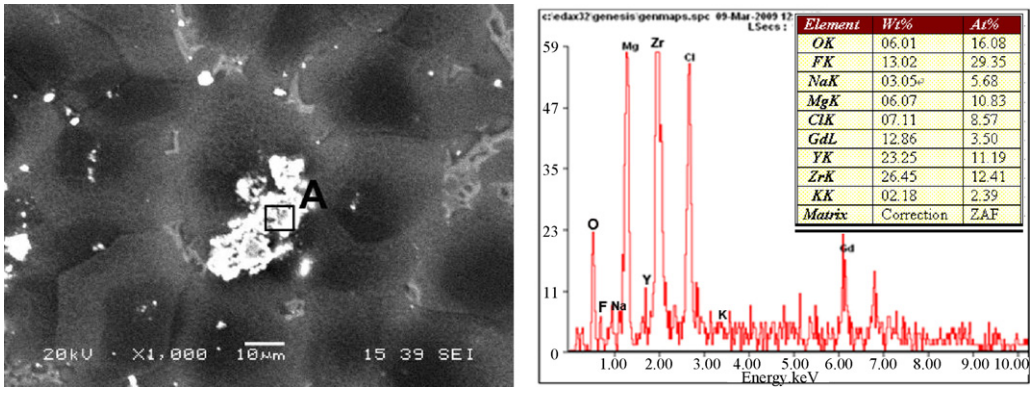

Fig. 11. SEM photographs and EDS result of salts mixture inclusion in GW103K alloy.

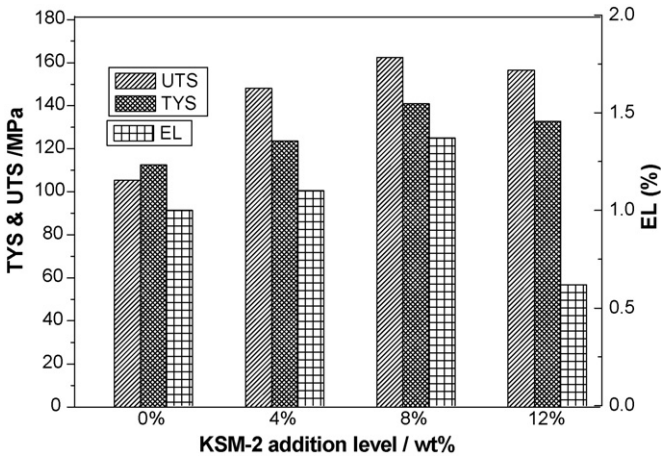

Fig. 12. Effect of KSM addition level on the tensile properties of GW103K alloy at room temperature.

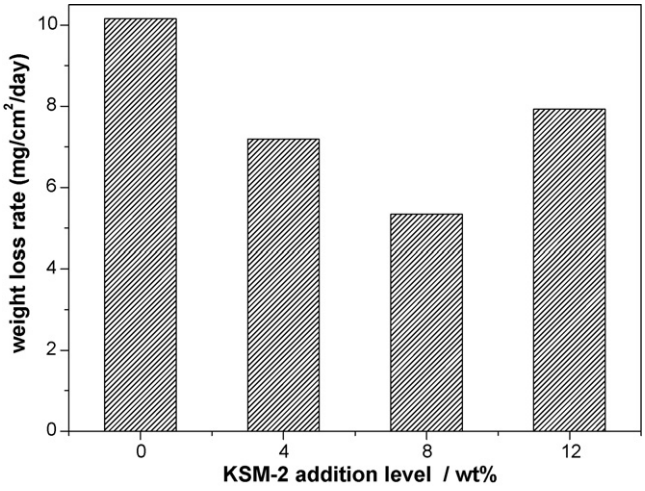

Fig. 13. Weight loss corrosion rate of GWK alloys after immersion for 3 days in 5 wt.% NaCl aqueous solution (pH 8.3, 25 ± 0.5 °C).

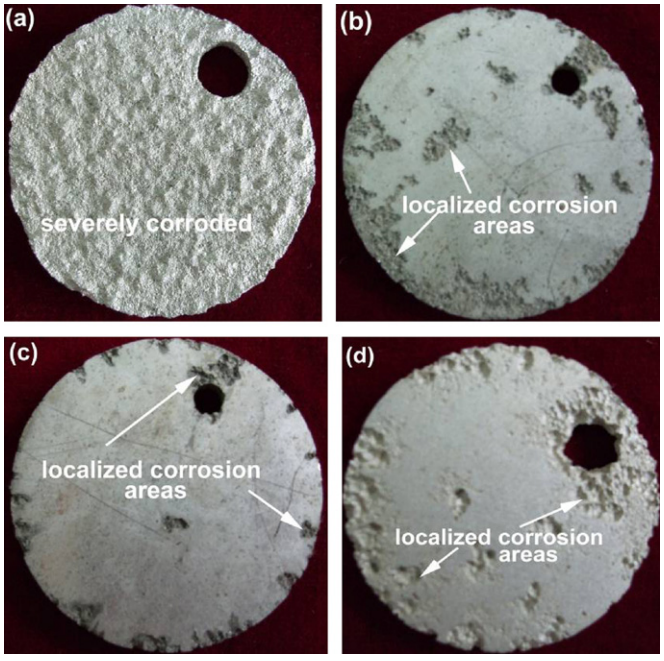

Fig. 14. The corroded surface photographs of GW103 alloys: (a) untreated; (b) 4% KSM-2 treated; (c) 8% KSM-2 treated; (d) 12% KSM-2 treated.

Table 3
Thermodynamic data of reaction (5).

Substance	Mg	ZrF_4	MgF_2	Zr
H^{Θ}_{298} (J mol^{-1} K^{-1})	0	−1,911,251	−1,123,404	0
ϕ_{1053} (J mol^{-1} K^{-1})	48.7063	168.6348	96.0235	54.0280

The L(KF, ZrF_4) has a melting point of about 470 °C [28], and it can react with Mg as Eq. (3). Simultaneously, Basile et al. [29] indicated that the compound K_3ZrF_7 is stable from room temperature up to 900 °C, but in the KCl–NaCl molten salts, K_3ZrF_7 is susceptible to decompose as Eq. (4), and the subsequent product ZrF_4 can reacts with Mg as Eq. (5):

$$L(KF, ZrF_4) + 2Mg = Zr + 2MgF_2 + KF \quad (3)$$

$$K_3ZrF_7 = 3KF + ZrF_4 \quad (4)$$

$$ZrF_4 + 2Mg = Zr + 2MgF_2 \quad (5)$$

Therefore, in KSM processed magnesium melt, reactions Eqs. (1)–(5) may take place. The ultimate reaction is Eq. (6), i.e. the sum of the former reactions (1)–(5). From Eqs. (1)–(5), it can be inferred that the ZrF_4 which formed from L(KF, ZrF_4) and K_3ZrF_7 is the main reaction substance that reacts with Mg.

$$K_2ZrF_6 + 2Mg = Zr + 2MgF_2 + 2KF \quad (6)$$

Generally, it is difficult to experimentally observe reactions that occur in a chemically complicated alloy melt. Therefore, we tried to analyze the reactions via thermodynamic calculations. Because of the instability of K_2ZrF_6 and lack of its thermo-chemical property data, we only calculate the change of Gibbs free energy of Eq. (5). The standard Gibbs free energy at the temperature of 780 °C (1053 K), ΔG^{Θ}_{1053}, can be calculated by Eq. (7), based on Gibbs free energy function (ϕ_T) method [30]:

$$\Delta G^{\Theta}_{1053} = \Delta H^{\Theta}_{298} - T\Delta\phi_{1053} \quad (7)$$

Using the standard ϕ_{1053} and H^{Θ}_{298} data of the substance shown in Table 3 [28,30], ΔG^{Θ}_{1053} of reaction (5) can be calculated as a value of −314526.0628 J mol^{-1}. The negative value of ΔG^{Θ}_{1053} indicates that reaction (5) can occur spontaneously under experimental conditions, and that thermodynamically the formation of Zr is favored. The reaction is further confirmed by the XRD result of the melting slag shown in Fig. 15, in which the products of KF, MgF_2 are present.

Density of solid state 50 wt.% NaCl–50 wt.% KCl is 2.08 g/cm^3, while that of liquid state (≥658 °C) is 1.5 g/cm^3 [23], which is a little lower than that of liquid Mg (~1.58 g/cm^3 at 650 °C). The liquid state

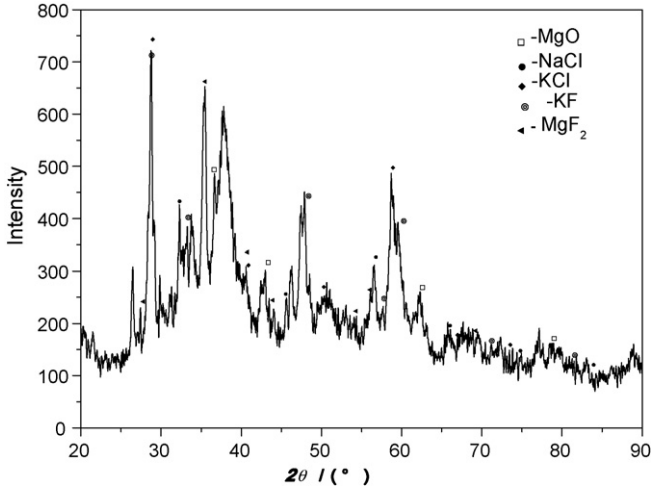

Fig. 15. XRD pattern of melting slag.

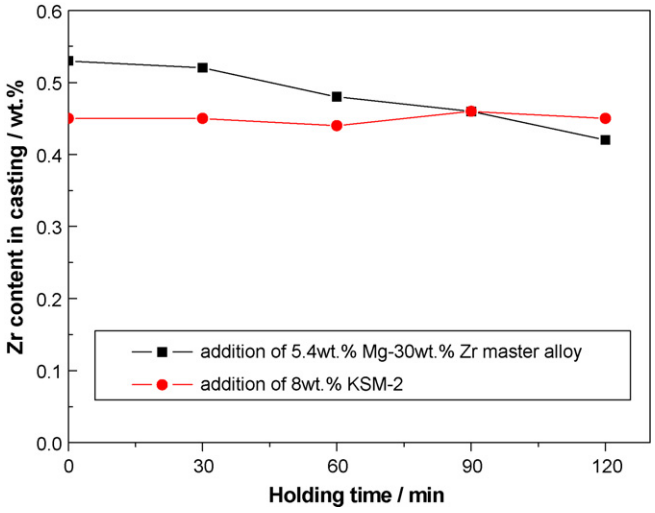

Fig. 16. Comparison of the fading time of grain refinement between the addition of 8 wt.% KSM-2 and that of 5.4 wt.% Mg–30 wt.%Zr master alloy. Industrially the latter can yield 0.4–0.6 wt.% Zr content in magnesium alloys.

densities at 780 °C of three KSM are measured as follows: 1.393, 1.462 and 1.539 g/cm^3, respectively, indicating that during smelting the residual salts mixture may not sink. In this paper, we do not adopt flux so as to better understand the formation of the inclusion to guide the future purification work. Melting points of KF and MgF_2 are 858 and 1266 °C [30], respectively, whilst density of KF and MgF_2 are 2.48 and 3.15 g/cm^3, respectively. At the experimental temperature (750–810 °C), the *in situ* KF and MgF_2 are of solid state, and both are much heavier than that of liquid Mg, so they are expected to sink down to the bottom of the crucible with increasing holding time. Nevertheless, in practical experimental condition, fraction of the *in situ* KF, MgF_2 may not be well separated from the salts mixture, thus forming the inclusions whose compositions mainly consist of fluorides and chlorides as shown in Fig. 11.

As shown in Fig. 16, with extending holding time to 120 min, the Zr content in GW103K refined by 8% KSM-2 almost keeps stable. However, the Zr content in GW103K refined by an addition of 5.4 wt.% Mg–30 wt.% Zr master alloy fades with increasing holding time. Industrially the latter can yield 0.4–0.6 wt.% Zr content in magnesium alloys.

Especially, it decreases much after 120 min, indicating that the grain refinement effect of Mg–Zr master alloy only last for a short time after addition [12]. Therefore, K_2ZrF_6 salts mixture refiner possesses much longer fading time comparing that of Mg–Zr master alloy, and this is similar with previous study on refining effect of salts containing Ti and B elements in purity aluminum compared with that of Al–Ti–B master alloy [31].

5. Conclusions

Based on the experimental results obtained in this work, the following conclusions could be drawn:

(1) K_2ZrF_6 salts mixture (KSM) is proved to be an effective grain refiner for GW103 magnesium alloy. Considering the grain size and volume fraction of inclusions, the 8% KSM-2 (50 wt.% K_2ZrF_6–25 wt.% NaCl–25 wt.% KCl) is the optimal grain refiner.
(2) The alloy refined by 8% KSM-2 has the highest tensile properties (UTS: 162.4 MPa; YS: 140.9 MPa; EL: 1.37%), and corrosion rate declines to the minimal 5.338 mg cm^{-2} day^{-1}.
(3) The reduction reaction between Mg and K_2ZrF_6 is responsible for grain refinement. Grain refinement effect of KSM can last for a long time, and its fading time can exceed 120 min.

Acknowledgements

The present study is funded by the National Basic Research Program of China (No. 2007CB613701), Program of Shanghai Subject Chief Scientist (No. 08XD14020) and Aerospace Science and Technology Innovation Fund of China Aerospace Science and Technology Corporation (No. 0502).

References

[1] S.M. He, X.Q. Zeng, L.M. Peng, X. Gao, J.F. Nie, W.J. Ding, J. Alloys Compd. 427 (2007) 316–323.
[2] X. Zhang, L. Li, Y. Deng, N. Zhou, J. Alloys Compd. 481 (2009) 296–300.
[3] C.J. Chen, Q.D. Wang, D.D. Yin, J. Alloys Compd. 487 (2009) 560–563.
[4] G. Yongchun, L. Jianping, L. Jinshan, Y. Zhong, Z. Juan, X. Feng, L. Minxian, J. Alloys Compd. 450 (2008) 446–451.
[5] W. Wang, HuangF Y., G. Wu, Q. Wang, M. Sun, W. Ding, J. Alloys Compd. 480 (2009) 386–391.
[6] X.B. Liu, R.S. Chen, E.H. Han, J. Alloys Compd. 465 (2008) 232–238.
[7] T. Honma, T. Ohkubo, S. Kamado, K. Hono, Acta Mater. 55 (2007) 4137–4150.
[8] M. Qian, Z.C.G. Hildebrand, D.H. StJohn, Metall. Mater. Trans. A 40A (2009) 2470–2479.
[9] G.B. Hamu, D. Eliezer, K.S. Shin, S. Cohen, J. Alloys Compd. 431 (2007) 269–276.
[10] G. Song, D. StJohn, J. Light Met. 2 (2002) 1–16.
[11] B.L. Mordike, Mater. Sci. Eng. A 324 (2002) 103–112.
[12] E.F. Horst, B.L. Mordike, Magnesium Technology: Metallurgy, Design Data, Application, Springer-Verlag, Berlin-Heidelberg, 2006, pp. 128.
[13] M. Qian, A. Das, Scripta Mater. 54 (2006) 881–886.
[14] W.C. Neil, M. Forsyth, P.C. Howlett, C.R. Hutchinson, B.R.W. Hinton, Corros. Sci. 51 (2009) 387–394.
[15] M. Sun, G.H. Wu, W. Wang, W.J. Ding, Mater. Sci. Eng. A 523 (2009) 145–151.
[16] P. Cao, M. Qian, D.H. StJohn, M.T. Frost, Mater. Sci. Technol. 20 (2004) 585–592.
[17] M. Qian, D. StJohn, M.T. Frost, Scripta Mater. 50 (2004) 1115–1119.
[18] M. Qian, D. StJohn, M.T. Frost, US Patent 0,161,121, 2005.
[19] M. Qian, D. St. John, M.T. Frost, in: H.J. Kaplan (Ed.), Magnesium Tech., TMS, Warrendale, PA, 2003, pp. 209–214.
[20] W. Unsworth, US Patent 2,970,904, 1961.
[21] M. Qian, L. Zheng, D. Graham, M.T. Frost, D.H. StJohn, J. Light Met. 1 (2001) 157–165.
[22] J.A.S. Tenório, D.C.R. Espinosa, in: G.E. Totten, D.S. MacKenzie (Eds.), Handbook of Aluminum (Vol. 2): Alloy Production and Materials Manufacturing, Marcel Dekker Inc., New York, 2003, pp. 128–130.
[23] B. Zhou, Y. Yang, M.A. Reuter, Proceedings Yazawa International Symposium on Metallurgical and Materials Processing, San Diego, California, USA, 2003, pp. 1249–1258.
[24] W. Wang, G.H. Wu, Q.D. Wang, Y.G. Huang, W.J. Ding, Mater. Sci. Eng. A 507 (2009) 207–214.
[25] M. Qian, D.H. StJohn, Int. J. Cast Met. Res. 22 (2009) 256–259.
[26] M. Qian, Acta Mater. 55 (2007) 943–953.
[27] S. Schamm, R. Fedou, J.P. Rocher, J.M. Quenisset, R. Naslain, Metall. Mater. Trans. A 22 (1991) 2133–2139.
[28] J.C. Cohen, US Patent 3,111,401, 1963.
[29] F. Basile, E. Chassaing, G. Lorthioir, J. Appl. Electrochem. 14 (1984) 731–739.
[30] D.L. Ye, J.H. Hu, Practical Handbook of Thermodynamic Data on Inorganic Substances (in Chinese), Second ed., Metallurgical Industry Press, Beijing, 2002.
[31] H.H. Zhang, X. Tang, G.J. Shao, L.P. Xu, J. Mater. Process. Technol. 180 (2006) 60–65.